Synthesis of heterometallic butterfly carbide clusters containing three different metals: (PPN)[$Fe_2CoM(dmpm)(CO)_{11}C$] (M = Mo or W)

Dean H. Johnston, Charlotte L. Stern and Duward F. Shriver*
Department of Chemistry, Northwestern University, Evanston, IL 60208 (USA)

(Received March 9, 1993)

Abstract

Cluster building reactions with the phosphine-substituted ketenylidene cluster (PPN)[$Fe_2Co(dmpm)(CO)_7CCO$] (**1**) provide a route to four-metal carbide clusters containing three different metals. The new clusters have the general formula (PPN)[$Fe_2CoM(dmpm)(CO)_{11}C$] (M = Mo (**2a**), W (**2b**)) and were characterized by IR spectroscopy, variable temperature NMR spectroscopy, FAB mass spectrometry, elemental analysis and, for M = W, a single crystal X-ray structure. The structure of (PPN)[$Fe_2CoW(dmpm)(CO)_{11}C$] (**2b**) consists of a 'butterfly' arrangement of the four metals around the carbide. The tungsten atom is located on the hinge, the cobalt atom is at one wingtip, and the dmpm ligand spans the cobalt–tungsten bond. Mechanisms for the formation of these products are discussed. Crystal data for **2b**: space group $P\bar{1}$, $a = 9.458(4)$, $b = 15.408(6)$, $c = 19.472(9)$ Å, $\alpha = 73.73(4)$, $\beta = 76.52(3)$, $\gamma = 83.56(3)°$, $V = 2646(3)$ Å^3, $Z = 2$.

Introduction

The ketenylidene clusters, $[M_3(CO)_9CCO]^{2-}$ (M = Fe, Ru, Os), are versatile precursors to four-, five- and six-metal heterometallic carbide clusters prepared via reaction of the anionic cluster with electrophilic cluster building reagents [1, 2]. The phosphine-substituted di-iron cobalt ketenylidene cluster (PPN)[$Fe_2Co(dmpm)(CO)_7CCO$] (**1**) (dmpm = bis(dimethylphosphino)methane) has been shown [3] to react with electrophiles in a manner analogous to the dianionic tri-iron ketenylidene cluster, $(PPN)_2[Fe_3(CO)_9CCO]$. This contrasts with the reactivity of $[Fe_2Co(CO)_9CCO]^-$, which is susceptible to nucleophilic attack [4]. The similarity in reactivity between $(PPN)_2[Fe_3(CO)_9CCO]$ and (PPN)[$Fe_2Co(dmpm)(CO)_7CCO$] has been ascribed [3] to the high degree of electron donation from the dmpm ligand.

In the present work the nucleophilicity of (PPN)[$Fe_2Co(dmpm)(CO)_7CCO$] is employed in cluster-building reactions leading to butterfly carbide clusters. This is the first cluster-building reaction reported on a ketenylidene cluster containing a diphosphine ligand. The rearrangement of the dmpm ligand which occurs in the course of the cluster-building reaction provides some hints on the cluster-building process.

*Author to whom correspondence should be addressed.

Experimental

Due to the air-sensitive nature of these anionic cluster compounds, all the following procedures were carried out under an atmosphere of purified nitrogen using standard Schlenk and syringe techniques [5]. All solvents, dichloromethane, acetone, acetonitrile, diethyl ether and pentane, were refluxed over appropriate drying agents and freshly distilled before use. Solids were manipulated under nitrogen in a glovebox.

Bis(dimethylphosphino)methane (dmpm), $Fe_3(CO)_{12}$, $Co_2(CO)_8$, $Mo(CO)_6$ and $W(CO)_6$ were used as supplied from Strem Chemicals. $Mo(CO)_3(NCMe)_3$ [6], $W(CO)_3(NCEt)_3$ [7] and (PPN)[$Fe_2Co(dmpm)(CO)_7$-CCO] [4] were synthesized using procedures described previously.

*Synthesis of (PPN)[$Fe_2CoMo(dmpm)(CO)_{11}C$] (**2a**)*

A Schlenk flask was loaded with 0.200 g (0.185 mmol) of (PPN)[$Fe_2Co(dmpm)(CO)_7CCO$] and 0.056 g (0.185 mmol) of $Mo(CO)_3(NCMe)_3$. Acetone (10 ml) was added and the solution was stirred for *c.* 20 min. The volume was reduced to 5 ml, and diethyl ether (10 ml) and pentane (20 ml) were added sequentially. The solvents were filtered off and the remaining oily solids were dried *in vacuo*. The black microcrystalline powder was redissolved in 10 ml of dichloromethane and layered with 60 ml of pentane. The resulting black needle

0020-1693/93/$6.00

crystals were collected by filtration, washed with 10 ml of pentane, and dried under vacuum. Yield 0.175 g isolated, 75%. IR (cm^{-1}, CH_2Cl_2): 2026s, 1971vs, 1954vs, 1916m, 1888w, 1843w. FAB-MS: peak at $m/z=725$ ($R=6.17$; $m/z=719$–727) with successive loss of four COs. *Anal.* Calc. for $C_{53}H_{44}CoFe_2MoNO_{11}P_4$: C, 50.46; H, 3.52; P, 9.82; Co, 4.67; Fe, 8.86; Mo, 7.61. Found: C, 50.20; H, 3.58; P, 9.41; Co, 4.70; Fe, 8.55; Mo, 7.42%.

Synthesis of (PPN)[$Fe_2CoW(dmpm)(CO)_{11}C$] (2b)

(PPN)[$Fe_2CoW(dmpm)(CO)_{11}C$] was synthesized using the procedures described above except 0.090 g (0.208 mmol) of $W(CO)_3(NCEt)_3$ was used, and the product was isolated in 81% yield. IR (cm^{-1}, CH_2Cl_2): 2059vw, 2026s, 1973vs, 1954vs, 1912m, 1893w, 1840w. FAB-MS: peak at $m/z=811$ ($R=8.95$; $m/z=809$–814) with successive loss of four COs.

Samples of both (PPN)[$Fe_2CoMo(dmpm)(CO)_{11}C$] and (PPN)[$Fe_2CoW(dmpm)(CO)_{11}C$] were isotopically enriched in ^{13}C at the carbide atom and all carbonyls by using isotopically enriched $(PPN)_2[Fe_3(CO)_9CCO]$, prepared as described earlier [8], as a starting material. Significant depletion of ^{13}CO occurred in the cluster building reactions so it was necessary to use $(PPN)_2[Fe_3(CO)_9CCO]$ enriched to levels of 40–50% ^{13}C to obtain products with convenient levels of isotopic enrichment for ^{13}C NMR spectroscopy.

Instrumentation

IR spectra for all compounds were measured at 2 cm^{-1} resolution using a Mattson Alpha Centauri FT-IR spectrometer equipped with a DTGS detector. Solution spectra were collected in cells with CaF_2 windows and a 0.1 mm path length. $^{13}C\{^1H\}$ and $^{31}P\{^1H\}$ NMR were recorded using a Varian XL-400 spectrometer operating at 100.577 or 161.905 MHz, respectively. ^{13}C chemical shifts are reported as downfield shifts from TMS using CD_2Cl_2 as an internal reference (53.80 ppm). $Cr(acac)_3$ (acac = acetylacetonate) was added to samples as a shiftless relaxation agent. ^{31}P chemical shifts are reported as shifts from an external 85% H_3PO_4 reference solution.

The liquid secondary ion (colloquially FAB) mass spectra were run on a VG-70 SE double-focusing high resolution mass spectrometer. Cesium iodide was used as the primary ion source, and *m*-nitrobenzyl alcohol (MNBA) was used as the matrix. The primary source current was 1 μA and 30 kV of ion beam was used to sputter the liquid sample surface. Negative ion detection was used to collect all the mass spectral data. Elemental analysis was performed by Elbach Analytical Laboratories, Gummersbach, Germany.

X-ray crystal structure of (PPN)[$Fe_2CoW(dmpm)(CO)_{11}C$] (2b)

Deep black crystals were grown by slow diffusion of a 1:1 diethyl ether/pentane mixture into a dichloromethane solution of the cluster. An opaque, plate-like crystal was cut from a larger crystal, mounted to a thin glass fiber in air, then transferred to the cold stream (−120 °C) of an Enraf-Nonius CAD4 diffractometer. A summary of the data collection is given in Table 1. The space group $P\bar{1}$ (No. 2) was confirmed by the average values of the normalized structure factors and the successful refinement of the proposed model in the centric space group.

The reflection intensities were very weak. The intensities of the three standard reflections were observed once per 1000 reflections measured. No significant crystal decay was observed. The data were corrected for Lorentz and polarization effects and anomalous dispersion effects [9]. A numerical absorption correction was applied with the resulting transmission factors ranging from 0.399 to 0.907.

The structure was solved using direct methods (SHELXS-86 [10]); correct positions for the tungsten, cobalt and iron were deduced from an *E*-map. Subsequent least-squares difference Fourier calculations revealed positions for the remaining non-hydrogen atoms. Hydrogen atoms were included as fixed contributors in 'idealized' positions. In the final least-squares refinement cycle, independent isotropic thermal coeffi-

TABLE 1. Crystal data for (PPN)[$Fe_2CoW(dmpm)(CO)_{11}C$]

Formula	$WCoFe_2P_4O_{11}NC_{53}H_{44}$
M	1349.31
Crystal size (mm)	0.03 × 0.30 × 0.30
Crystal system	triclinic
Space group	$P\bar{1}$
a (Å)	9.458(4)
b (Å)	15.408(6)
c (Å)	19.472(9)
α (°)	73.73(4)
β (°)	76.52(3)
γ (°)	83.56(3)
V (Å^3)	2646(3)
Z	2
D_{calc} (g cm^{-3})	1.693
μ (Mo Kα) (cm^{-1})	32.36
Radiation	Mo Kα ($\lambda=0.71073$ Å, graphite monochromated)
T (°C)	−120
Scan type	ω/θ
2θ range (°)	2–46
Unique data	7342
Unique data, $I>2.58\sigma(I)$	4090
No. parameters	570
$R(F)$[a]	0.056
$R_w(F)$[b]	0.067

[a] $R(F)=[\Sigma||F_o|-|F_c||/\Sigma|F_o|]$. [b] $R_w(F)=[\Sigma w(|F_o|-|F_c|)^2/\Sigma wF_o^2]^{1/2}$, $w=4F_o^2/\sigma^2(F_o^2)$.

TABLE 2. Positional parameters for the cluster anion of (PPN)[$Fe_2CoW(dmpm)(CO)_{11}C$]

Atom	x	y	z
W	0.32401(8)	0.85697(5)	0.65395(4)
Co	0.2877(2)	0.8671(2)	0.7984(1)
Fe1	0.1087(2)	0.6775(2)	0.7663(1)
Fe2	0.3322(3)	0.6675(2)	0.7311(1)
P1	0.5912(5)	0.8724(3)	0.6392(3)
P2	0.5146(5)	0.8717(4)	0.8011(3)
O2	0.433(1)	0.7869(8)	0.5125(7)
O3	0.029(1)	0.9076(8)	0.6013(7)
O4	0.320(1)	1.0677(9)	0.5865(7)
O5	0.140(1)	0.8380(9)	0.9508(7)
O6	0.212(1)	1.0606(8)	0.7464(7)
O7	−0.080(1)	0.9369(9)	0.7777(7)
O8	−0.044(1)	0.6854(9)	0.6932(8)
O9	−0.006(1)	0.6669(10)	0.9142(8)
O10	0.273(1)	0.6067(10)	0.6099(7)
O11	0.226(2)	0.5230(9)	0.8596(8)
O12	0.635(1)	0.6066(9)	0.7229(8)
C1	0.319(2)	0.770(1)	0.7600(9)
C2	0.392(2)	0.812(1)	0.5634(9)
C3	0.135(2)	0.883(1)	0.6261(10)
C4	0.325(2)	0.992(1)	0.6111(9)
C5	0.201(2)	0.847(1)	0.891(1)
C6	0.244(2)	0.984(1)	0.7660(10)
C7	−0.003(2)	0.876(1)	0.773(1)
C8	0.017(2)	0.721(1)	0.723(1)
C9	0.041(2)	0.711(1)	0.857(1)
C10	0.297(2)	0.630(1)	0.6575(10)
C11	0.266(2)	0.579(1)	0.807(1)
C12	0.517(2)	0.633(1)	0.723(1)
C30	0.651(2)	0.840(1)	0.7256(8)
C31	0.660(2)	0.986(1)	0.597(1)
C32	0.722(2)	0.805(1)	0.5859(9)
C33	0.565(2)	0.984(1)	0.800(1)
C34	0.579(2)	0.801(1)	0.880(1)

cients were refined for carbon atoms, a common isotropic thermal parameter was varied for the hydrogen atoms, anisotropic thermal coefficients were refined for the remaining non-hydrogen atoms and an empirical extinction parameter was refined to a value of $1.6(8)\times10^{-8}$. Successful convergence was indicated by the maximum shift/error for the final cycle. The highest peaks in the final difference Fourier map were in the vicinity of the metal atoms. A final analysis of variance between observed and calculated structure factors showed no apparent systematic errors. The positional parameters for the cluster anion of (PPN)[$Fe_2CoW(dmpm)(CO)_{11}C$] are given in Table 2.

Results and discussion

The dmpm-substituted di-iron cobalt ketenylidene, (PPN)[$Fe_2Co(dmpm)(CO)_7CCO$] (**1**), is shown here to be a useful precursor for the preparation of butterfly carbide clusters containing three different metals. The reactivity of **1** toward electrophilic cluster building reagents is analogous to that of other anionic ketenylidenes, but displays several differences. Reaction of (PPN)[$Fe_2Co(dmpm)(CO)_7CCO$] with $M(CO)_3(NCR)_3$ (M = Mo or W) results in the formation of clusters with nuclearity no higher than four, even in the presence of excess $M(CO)_3(NCMe)_3$. This is in contrast to the Fe, Ru and Os ketenylidenes, which upon reaction with $M(CO)_3(NCMe)_3$ either form both four- and five-metal carbides (Fe [1]), or exclusively five-metal carbides (Ru, Os [2]). In this work, attempts to prepare the Cr-containing cluster resulted in the isolation of a product containing a mixture of four- and five-metal clusters.

IR spectroscopy is a very sensitive tool to monitor these cluster building reactions. The low symmetry of the product in this case leads to a complex absorption pattern in the ν(CO) region which can be used as a 'fingerprint' to monitor the course of a reaction and identify products. The nearly identical ν(CO) absorption patterns for (PPN)[$Fe_2CoW(dmpm)(CO)_{11}C$] (M = Mo or W) indicate these two products are isostructural. IR was also used to tentatively identify the unstable products that were not isolated.

The FAB mass spectra also confirmed the proposed formulations. Peaks were observed at *m/z* ratios that corresponded to the expected parent ions, displayed the proper isotope distributions, and showed successive loss of COs. *R* factors (analogous to crystallographic *R* factors) were calculated for the mass ranges listed as described previously [11, 12] and confirmed the assignments. Peaks of higher mass in the FAB mass spectra corresponded to a single cluster paired with a molecule of the MNBA (*m*-nitrobenzyl alcohol) matrix. Successive loss of at least eight COs from the cluster-matrix pair was observed, with the most intense peak in both cases corresponding to loss of four COs.

Variable temperature multinuclear (^{13}C and ^{31}P) NMR was the most useful technique in determining the composition and structure of these clusters. A summary of the NMR data is given in Table 3. The ^{31}P NMR data indicate chelation of the dmpm ligand across a Co–M bond, where M = Mo or W. Two (non-PPN^+) resonances are observed at 25 °C for (PPN)[$Fe_2CoMo(dmpm)(CO)_{11}C$], one broad resonance at 27.4 ppm and a second sharp doublet (J_{PP} = 77 Hz) at −6.4 ppm. Upon lowering the temperature to −90 °C, the broad resonance sharpens to a doublet (J_{PP} = 73 Hz). The broad resonance is due to phosphorus coordinated to the quadrapolar Co atom. The ambiguity in the coordination of the second phosphorus atom is removed upon inspection of the ^{31}P spectrum of (PPN)[$Fe_2CoW(dmpm)(CO)_{11}C$]. At 25 °C, a broad resonance is observed at 26.3 ppm similar to the ^{31}P

TABLE 3. Variable temperature $^{13}C\{^1H\}$ and $^{31}P\{^1H\}$ NMR data on (PPN)[$Fe_2CoM(dmpm)(CO)_{11}C$], M = Mo or W[a]

Heterometal (M)	Nucleus	Temp.	Chemical shift data[b,c]
Mo	^{13}C	+25	491.85 (carbide, d, $^2J_{CP}$ = 10 Hz), 220.7, 212.8 (br), 205.5 (br)
Mo	^{13}C	−90	492.6 (carbide), 237.7 (1), 232.3 (1), 229.0 (1), 221.0 (3), 220.6 (1), 219.1 (1), 213.3 (1), 212.5 (1), 205.4 (1)
Mo	^{31}P	+25	+27.4 (br), −6.4 (d, J_{PP} = 77 Hz)
Mo	^{31}P	−90	+27.5 (d, J_{PP} = 73 Hz), −6.7 (d, J_{PP} = 72 Hz)
W	^{13}C	+25	491.7 (carbide, dws, $^2J_{CP}$ = 11 Hz, J_{CW} = 30 Hz), 230 (br), 224 (br), 220.1, 219 (br), 211 (br), 208.9, 201.4
W	^{13}C	−30	491.6 (carbide, dws, $^2J_{CP}$ = 11 Hz, J_{CW} = 30 Hz), 230.5 (1, sws, J_{CW} = 130 Hz), 224.4 (1, m, J_{CW} = 145 Hz, $^5J_{CP}$ = 8 Hz), 223.0 (1, m, J_{CW} = 130 Hz, J_{CC} = 6 Hz), 220.3 (1), 219.7 (3), 218.6 (1), 210.8 (1, t, J_{CC} = 7 Hz), 208.5 (1, br), 200.9 (1, d, br, $^5J_{CP}$ = 6 Hz)
W	^{31}P	+25	+26.3 (br), −30.1 (dws, J_{PP} = 75 Hz, J_{PW} = 212 Hz, $^2J_{PC}$ = 10 Hz)

[a]Spectra recorded in CD_2Cl_2. [b]Values given in ppm; ^{13}C data listed as downfield shifts; from TMS; ^{31}P data listed as shifts from 85% H_3PO_4. Values in parentheses are integrated intensities for carbonyl resonances. [c]Key to abbreviations: br = broad, d = doublet, t = triplet, sws = singlet with ^{183}W satellites, dws = doublet with ^{183}W satellites, m = multiplet, ^2J = two-bond coupling, ^5J = through-space coupling.

spectrum of **2a**, but a sharp doublet is observed at −30.1 ppm which has ^{183}W satellites indicating the dmpm ligand is coordinated to the tungsten atom. The measured coupling constants, J_{PP} = 75 Hz and J_{PW} = 212 Hz, agree with a previously characterized compound, FeCoWCp(dmpm)$(CO)_8$(PMe) [13], containing a Co–W bond spanned by a dmpm ligand where J_{PP} = 104 Hz and J_{PW} = 214 Hz.

The variable temperature ^{13}C NMR spectra of (PPN)[$Fe_2CoM(dmpm)(CO)_{11}C$] (M = Mo or W) contain a large amount of structural information. The carbonyls in the molybdenum-containing cluster appear to be slightly more fluxional. The spectrum of **2a** at room temperature displays only one sharp peak (assigned to the wingtip iron carbonyls) and a few broad resonances. The spectrum of **2b**, on the other hand, contains broad features of every peak found in the low temperature spectrum. The carbide resonances for both clusters have clear two-bond coupling (J_{CP} = ~10 Hz) of the carbide to a phosphorus of the dmpm ligand. Two-bond coupling of this type has been observed previously [2] between the carbide and wingtip carbonyl ligands in similar butterfly carbide clusters. In the case of the tungsten containing cluster, the carbide resonance at 491.6 ppm displays satellites (J_{CW} = 30 Hz) due to coupling of the carbide atom to the hinge tungsten atom. This coupling constant is slightly less than the carbide–hinge-tungsten coupling constant of 50 Hz observed for $[Fe_3W(CO)_{13}C]^{2-}$ [1]. It is significantly less than the coupling constant of 80 Hz observed for $[WRu_3(\eta\text{-}C_5H_5)(CO)_{11}(\mu_4\text{-}C)(\mu\text{-}H)]$, where the tungsten atom occupies the hinge position [14]. The larger coupling observed for $[WRu_3(\eta\text{-}C_5H_5)(CO)_{11}(\mu_4\text{-}C)(\mu\text{-}H)]$ is presumably due to the strong wingtip metal to carbide bonding interaction [15].

Due to the close similarity between the ^{13}C NMR spectra of the two clusters and the greater amount of information in the spectra of **2b**, only the low temperature spectra of **2b** will be discussed in detail. The low temperature (−30 °C) ^{13}C spectrum and corresponding assignments are shown in Fig. 1. At room temperature, the broad resonances for the carbonyl ligands on the hinge metals indicates an exchange process between the carbonyls on each metal, and possibly between the metals. This is not unlikely as one of the hinge metal carbonyls often occupies a bridging or semi-bridging position across the hinge in butterfly carbide clusters. As the temperature is lowered,

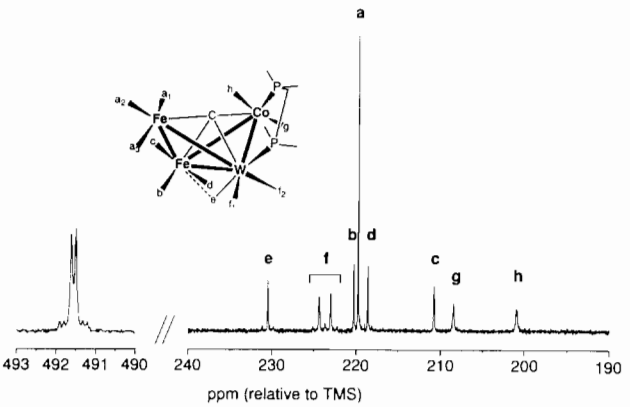

Fig. 1. ^{13}C NMR spectrum of isotopically enriched (PPN)[$Fe_2CoW(dmpm)(CO)_{11}C$] at −30 °C. Only the carbide and carbonyl resonances are shown. The inset structure shows assignments for each of the carbonyl resonances.

the hinge-iron carbonyl resonances sharpen considerably, while the hinge-tungsten carbonyl resonances show distinct peaks, but remain broad. At −30 °C, all the peaks are well resolved, and no improvement is seen at lower temperature (down to −90 °C). Of the nine carbonyl resonances, eight integrate to one and one integrates to three, accounting for all eleven carbonyl ligands in the structure.

Three of the carbonyl resonances show clear satellites due to coupling to the 14.3% abundant spin 1/2 ^{183}W nucleus. The most downfield of these peaks is assigned to the carbonyl in a semi-bridging position over the tungsten–iron hinge bond. The two remaining tungsten-bound carbonyl resonances cannot be definitively assigned, but both display fine splitting that may be due to through-space coupling to the phosphorus or two-bond coupling to the carbide atom. The sharp peak at 219.7 ppm that integrates to three carbonyls may clearly be assigned to the three wingtip-iron carbonyls that, due to turnstile rotation, remain equivalent down to −90 °C. The two broader upfield carbonyl resonances are assigned to cobalt-bound carbonyl ligands, the broadening being due to the interaction with the quadrapolar Co nucleus. The more deshielded resonance is assigned [3, 16] to the carbonyl ligand axially bound relative to the Co–W–Fe triangle.

The three remaining carbonyl ligand resonances are assigned to the hinge-iron atom. The upfield resonance displays very fine (7 Hz) splitting that may be due to through-space coupling to the carbide atom and is therefore assigned to the carbonyl ligand situated closest to the carbide. The other two carbonyl ligands are in nearly identical environments and display very similar shifts. Those resonances are therefore arbitrarily assigned in Fig. 1.

It is notable that the downfield shift observed (~490 ppm downfield from TMS) for the carbide atom in these clusters is the largest for any known carbide cluster of any geometry. Deshielding of interstitial atoms in transition metal clusters has been correlated to the 'compression' of the interstitial atom [17]. Calculation of the atomic radii for the interstitial carbide in the structurally characterized (PPN)[$Fe_2CoW(dmpm)(CO)_{11}C$] gives $r(C) = 54.6$ pm. This is smaller than the radii calculated for other transition metal carbides and, thus, the correlation appears to hold for this particular example.

An ORTEP diagram of the structure of the cluster anion of **2b** is shown in Fig. 2. The structure consists of a central μ_4-carbide coordinated by four metal atoms in a 'butterfly' configuration. One iron atom and the tungsten atom form the hinge, and the other iron atom and the cobalt are at the wingtips. The dihedral angle formed at the hinge of the butterfly is 100°, similar to the angle found in other butterfly carbide clusters [2, 14, 18]. The dmpm ligand spans the Co–W bond in an equatorial position relative to the Fe1–Co–W triangle. The carbonyls are arranged with three on each of the iron atoms, two on the cobalt atom and three on the tungsten atom. One of the carbonyls (C3–O3) on the tungsten atom is semi-bridging across the W–Fe1 bond resulting in a slight bend (171°) in the W–C3–O3 bond. A bridging or semi-bridging carbonyl ligand has been observed across the hinge bond in other structurally characterized butterfly carbide clusters [1, 2].

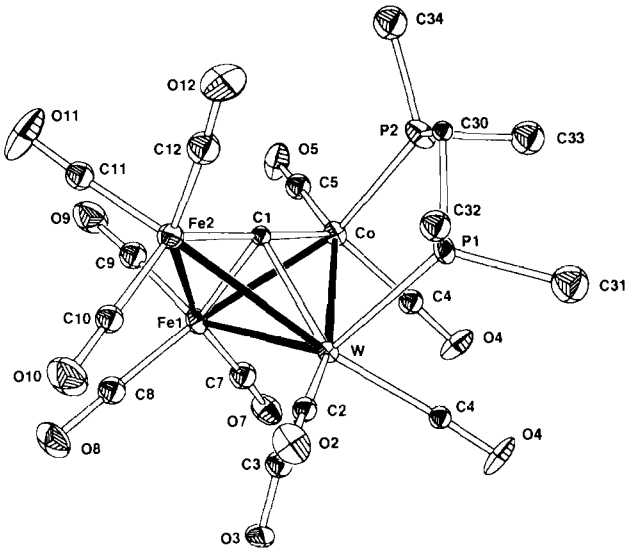

Fig. 2. An ORTEP diagram of the cluster anion of (PPN)[$Fe_2CoW(dmpm)(CO)_{11}C$]. Thermal ellipsoids are drawn at 35% probability. Hydrogen atoms are omitted for clarity.

Direct comparisons between the structure of (PPN)[$Fe_2CoW(dmpm)(CO)_{11}C$] and (PPN)[$Fe_2Co(dmpm)(CO)_7CCO$] cannot be made as the Fe_2Co triangle is not intact and the dmpm ligand no longer spans an iron–cobalt bond. The dmpm ligand spans a longer (Co–W) bond and therefore the P1–C31–P2 angle is slightly larger (112.9°) compared to 109.9° in **1**. The W(dmpm)Co portion of the cluster is very similar to the structure of $FeCoWCp(dmpm)(CO)_8(PMe)$ [13] in which the dmpm ligand also spans the Co–W bond. The Co–W bond length is the same within experimental error. The W–P(dmpm) bond length is slightly longer and the Co–P(dmpm) bond length is slightly shorter in **2b**.

The strong interaction between the carbide and the wingtip metals in **2b** results in a carbide–wingtip–metal bond length (Fe2–C1 = 1.80 Å) that is significantly shorter than carbide–hinge-metal distance (Fe1–C1 = 1.96 Å) (Table 4). This shortening has been observed in both homo [15] and heterometallic [1] iron butterfly carbide clusters and an Os_3Mn carbide cluster [2] as well. The iron–carbide distances found in **2b** are identical to the average distances found in the homometallic

TABLE 4. Selected bond distances (Å) and angles (°) for (PPN)[$Fe_2CoW(dmpm)(CO)_{11}C$]

Bond distances			
W–Fe2	2.887(3)	Fe1–C7	1.76(2)
W–Co	2.799(2)	Fe1–C8	1.76(2)
W–Fe1	2.724(3)	Fe1–C9	1.78(2)
Fe1–Fe2	2.640(3)	Fe2–C10	1.79(2)
Co–Fe1	2.584(3)	Fe2–C11	1.75(2)
W–C1	2.12(2)	Fe2–C12	1.76(2)
Fe1–C1	1.96(1)	C2–O2	1.13(2)
Co–C1	1.83(2)	C3–O3	1.20(2)
Fe2–C1	1.80(2)	C4–O4	1.13(2)
W–P1	2.506(4)	C5–O5	1.15(2)
Co–P2	2.168(5)	P1–C30	1.82(2)
W–C2	2.01(2)	P2–C30	1.86(2)
W–C3	1.95(2)	P1–C31	1.83(2)
W–C4	2.01(2)	P1–C32	1.85(2)
Co–C5	1.76(2)	P2–C33	1.84(2)
Co–C6	1.77(2)	P2–C34	1.80(2)
Bond angles			
W–Fe1–Fe2	65.09(8)	Co–C1–Fe1	86.1(6)
Fe1–W–Fe2	56.04(7)	Co–C1–Fe2	172.9(10)
W–Fe2–Fe1	58.87(8)	Fe1–C1–Fe2	89.3(6)
W–Fe1–Co	63.58(8)	W–C2–O2	179(1)
Fe1–Co–W	60.65(8)	W–C3–O3	171(1)
Co–W–Fe1	55.77(7)	W–C4–O4	177(1)
Co–Fe1–Fe2	87.53(10)	Co–C5–O5	176(2)
Co–W–Fe2	78.92(8)	W–P1–C30	113.2(5)
W–C1–Co	90.1(6)	Co–P2–C30	116.4(5)
W–C1–Fe1	83.7(6)	P1–C30–P2	112.9(8)
W–C1–Fe2	94.7(7)		

butterfly carbide cluster, $[Fe_4(CO)_{12}C]^{2-}$. The heteroatom (tungsten) is located on the hinge of the butterfly cluster in **2b** as has been observed for other heterometallic butterfly carbide clusters [1, 2].

Other attempts to synthesize higher nuclearity carbide clusters from **1** led to inseparable mixtures or unstable products. Reaction of **1** with excess $Cr(CO)_3(NCMe)_3$ appeared to yield a mixture of products, presumably four- and five-metal clusters. Previous work with Fe_3Cr and Fe_3Cr_2 carbide clusters [1] indicated facile interconversion between the four- and five-metal clusters and this interconversion presented difficulties in isolating pure products. Reaction of **1** with $[Mn(CO)_3(NCMe)_3](PF_6)$ yielded an apparently neutral product that was a mixture of at least two products as determined by ^{13}C NMR. The cluster-building reagent, $[Rh(CO)_2Cl]_2$, appeared by IR spectroscopy to react cleanly with **1**, but the product decomposed when isolation was attempted.

An interesting rearrangement was observed when the product from the reaction of **1** with $Cr(CO)_3(NCMe)_3$ was stirred under an atmosphere of 99% ^{13}CO for 24 h. A ^{13}C NMR spectrum of the product shows that the ketenylidene cluster is regenerated, but approximately 40% of the ketenylidene now has the dmpm ligand spanning the iron–iron bond. This new product has a plane of symmetry (whereas **1** has C_1 symmetry) resulting in a 2:2:2:1 pattern in the carbonyl region of the low temperature ^{13}C NMR spectrum. Some heterometallic four-metal carbide clusters are known to regenerate the ketenylidene starting material in the coordinating solvent CH_3CN [1]. Rearrangements of disphosphine ligands have also been shown to occur on similar clusters upon protonation, though the reason is unclear [19]. In the present case, it is not certain when the dmpm ligand rearranges, though it can be seen from the structure of **2b** that some rearrangement occurs in the cluster building step. It is unlikely that the rearrangement is due solely to the presence of carbon monoxide as decomposition is observed upon stirring a solution of **1** under an atmosphere of CO. Compound **2a** also decomposes under CO.

It is interesting to use the structures of **2a** and **2b** as a basis for speculation about the mechanism of the formation of heterometallic butterfly carbide clusters. Consider first the less complex case of cluster-building with the homometallic ketenylidene, $[M_3(CO)_9CCO]^{2-}$. In Scheme 1, all the carbonyl ligands on the ketenylidene cluster have been removed, leaving a M_3C tetrahedron. Addition of a heterometal (electrophilic metal fragment) may occur on either an MMC or MMM face. Both types of attachment have been observed in the interaction of ketenylidene clusters with electrophilic copper fragments [20, 21]. Neither intermediate, however, has the heterometal in the hinge position of a butterfly cluster, as does the product. Scheme 1 illustrates how both intermediates may undergo a diamond-square-diamond (DSD) [22] rearrangement, first breaking a metal–metal bond, then forming a new metal–metal or metal–carbon bond, to yield equivalent products. As the products from each case are indistinguishable, the simple homometallic ketenylidene case does not indicate a preference for one mechanism over the other.

Attack on the MMM face was previously invoked [18] with the thought that this route would require less rearrangement to place the heterometal on the hinge. However, Scheme 1 shows that either site of attack can lead to the product through equivalent rearrange-

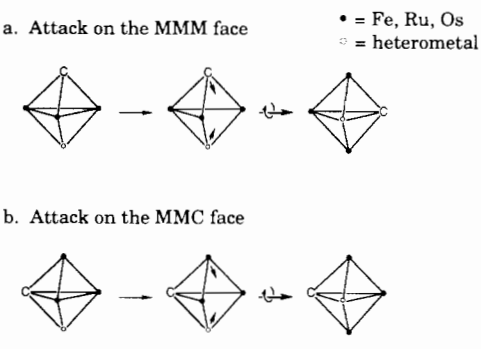

Scheme 1.

ments. The total number of metal–metal and metal–carbon bonds formed and broken in the overall processes are also equivalent. A mechanism similar to that shown in Scheme 1(b) has been proposed [23] to explain the hinge/wingtip isomerization of $[FeRu_3N(CO)_{12}]^-$. A second mechanism proposed [23] for the isomerization of $[FeRu_3N(CO)_{12}]^-$, which is not considered here, requires the cleavage and formation of twice as many bonds as the first mechanism to accomplish the same overall exchange.

Due to the low symmetry of $[Fe_2Co(dmpm)(CO)_7CCO]^-$, numerous reaction paths are possible. Indeed, clusters **1**, **2a** and **2b** all contain tetrahedrane (or larger) units with four different vertices and are therefore chiral. While other authors have elegantly explored the synthesis and properties of chiral organometallic clusters [24], no attempt was made in the present work to exploit this property. Scheme 2 illustrates attack on only one of the two possible enantiomers of **1**. One mechanism not considered in Scheme 2 is attack on the Fe(P)Co(P)C face which is sterically blocked by the rigid dmpm ligand. Attack on the other two sides [FeCo(P)C or FeFe(P)C] followed by a DSD rearrangement is diagrammed in Scheme 2(a) and (b). Neither of these rearrangements disrupt the Fe(P)–Co(P) bond, and in the product the dmpm remains coordinated across the Fe–Co bond. Similarly, as illustrated in Scheme 2(c) and (d), attack on the bottom face followed by cleavage of the Co(P)–Fe or Fe(P)–Fe bond does not disrupt the coordination of the dmpm ligand. The rearrangement shown in Scheme 2(e), however, involves cleavage of the Fe(P)–Co(P) bond and the dmpm ligand is forced to partially detach and recoordinate to a different metal. In addition, Scheme 2(e) places the Co atom at the wingtip (unlike Scheme 2(b) and (d)) as is found in the structure of **2b**. Scheme 2(e) is therefore proposed as the most likely mechanism by which the heterometallic butterfly carbides, **2a** and **2b**, are formed.

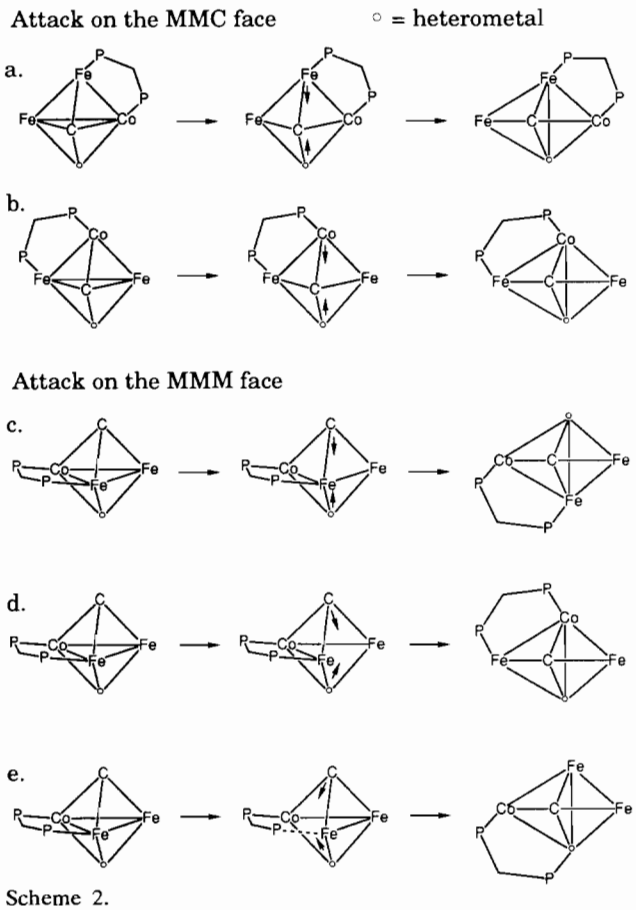

Scheme 2.

Supplementary material

Tables of X-ray crystallographic data for (PPN)-$[Fe_2CoW(dmpm)(CO)_{11}C]$, including complete refined positional parameters, anisotropic thermal parameters, bond distances, bond angles, and observed and calculated structure factors (34 pages) are available from the authors upon request.

Acknowledgements

This research was supported by DOE Grant DE-FG02-86ER13640. We thank Daphne Cody for assistance with the synthetic work, Gail Karet for helpful discussions concerning the mechanism, and Dr H. Hung for mass spectral analyses.

References

1 J.A. Hriljac, E.M. Holt and D.F. Shriver, *Inorg. Chem., 26* (1987) 2943.
2 M.P. Jensen, W. Henderson, D.H. Johnston, M. Sabat and D.F. Shriver, *J. Organomet. Chem., 394* (1990) 121.
3 S. Ching, M. Sabat and D.F. Shriver, *Organometallics, 8* (1989) 1047.
4 S. Ching, E.M. Holt, J.W. Kolis and D.F. Shriver, *Organometallics, 7* (1988) 892.
5 D.F. Shriver and M.A. Drezdzon, *The Manipulation of Air-Sensitive Compounds,* Wiley, New York, 2nd edn., 1986.
6 D.P. Tate, W.R. Knipple and J.M. Augl, *Inorg. Chem., 1* (1962) 433.
7 G.J. Kubas, *Inorg. Chem., 22* (1983) 692.
8 J.A. Hriljac and D.F. Shriver, *J. Am. Chem. Soc., 109* (1987) 6010.
9 J.A. Ibers and W.C. Hamilton (eds.), *International Tables for X-ray Crystallography,* Vol. IV, Kynoch, Birmingham, UK, 1974.
10 G.M. Sheldrick, in G.M. Sheldrick, C. Kruger and R. Goddard (eds.), *Crystallographic Computing,* Oxford University Press, London, 1985, p. 175.

11 M.A. Andrews, S.W. Kirtley and H.D. Kaesz, *Inorg. Chem., 16* (1977) 1556.
12 D.H. Johnston, D.C. Gaswick, M.C. Lonergan, C.L. Stern and D.F. Shriver, *Inorg. Chem., 31* (1992) 1869.
13 R.P. Planalp and H. Vahrenkamp, *Z. Naturforsch., B, 44* (1989) 139.
14 Y. Chi, S.-H. Chuang, B.-F. Chen, S.-M. Peng and G.-H. Lee, *J. Chem. Soc., Dalton Trans.,* (1990) 3033.
15 S. Harris and J.S. Bradley, *Organometallics, 3* (1984) 1086.
16 S. Aime, L. Milone, R. Rossetti and P.L. Stanghellini, *Inorg. Chim. Acta, 25* (1977) 103.
17 J. Mason, *J. Am. Chem. Soc., 113* (1991) 24.
18 J.A. Hriljac, P.N. Swepston and D.F. Shriver, *Organometallics, 4* (1985) 158.
19 S. Ching, M.P. Jensen, M. Sabat and D.F. Shriver, *Organometallics, 8* (1989) 1058.
20 A.S. Gunale, M.P. Jensen, C.L. Stern and D.F. Shriver, *J. Am. Chem. Soc., 113* (1991) 1458.
21 A.S. Gunale, M.P. Jensen, D.A. Phillips, C.L. Stern and D.F. Shriver, *Inorg. Chem., 31* (1992) 2622.
22 A. Rodger and B.F.G. Johnson, *Polyhedron, 7* (1988) 1107.
23 D.E. Fjare and W.L. Gladfelter, *J. Am. Chem. Soc., 106* (1984) 4799.
24 H. Vahrenkamp, *J. Organomet. Chem., 370* (1989) 65.